Monte Carlo Simulation of D-D Neutron Emission Rate in NBI-Heated Deuterium Plasma of LHD*)

Yutaka MATSUMOTO, Takafumi HOMMA[1)], Ryosuke SEKI[2,3)], Masaki OSAKABE[2,3)], Kunihiro OGAWA[2,3)] and Mitsutaka ISOBE[2,3)]

Faculty of Engineering, Hokkaido University, Sapporo 060-8628, Japan
[1)]*Graduate School of Engineering, Hokkaido University, Sapporo 060-8628, Japan*
[2)]*National Institute for Fusion Science, National Institute of National Sciences, Toki 509-5292, Japan*
[3)]*The Graduate University for Advanced Studies, SOKENDAI, Toki 509-5292, Japan*

(Received 10 January 2022 / Accepted 29 March 2022)

As the first step to analyze the orbit of the triton produced by the fusion reaction between the beam-injected deuteron and the deuteron in the bulk plasma, we developed the code to calculate the velocity and spatial profiles of the fusion products in the Large Helical Device (LHD) that properly treats the particle loss boundary and the velocity anisotropy of the triton at birth. The neutron emission and neutron counting rates calculated by the code were compared with experimental results. The experimental results are reproduced by the developed code when the bulk plasma density, including the impurity ion, was used.

Keywords: Monte-Carlo simulation, neutron emission rate, NBI, LHD

DOI: 10.1585/pfr.17.2403060

1. Introduction

The deuterium plasma experiment has been conducted in the Large Helical Device (LHD) since 2017 [1–4]. In the experiment, neutrons produced in the nuclear fusion reaction between the neutral beam (NB)-injected deuteron (D) and D in the bulk plasma are measured by an integrated set of neutron diagnostics, e.g., the neutron flux monitor and the vertical neutron camera (VNC) [5]. Secondary neutrons obtained from the nuclear fusion reaction between triton (T) produced by the D-D reaction and D in the bulk plasma are observed [6].

Measurements of the neutron emission rate and its spatial profile allow us to investigate the orbit properties of energetic ions, such as the NB-injected D ($\sim 100\,\mathrm{keV}$) and the DD-produced T ($\sim 1\,\mathrm{MeV}$). The properties of such energetic ions are highly important as they play significant roles not only in heating the bulk plasma but also in causing the nuclear fusion reaction. In particular, the importance of DD-produced T is highlighted because the Larmor radius of the DD-produced T is approximately the same as that of the α particle in D-T reactors. Therefore, the examination of fusion-produced neutrons is considered to be one of the most important issues in nuclear fusion research.

Numerical studies of fusion-produced T have been implemented using codes based on the magnetic coordinate system such as GNET [7–9]. The triton burnup ratio, the ratio of the neutron yield in the D-T fusion reaction to that in the D-D fusion reaction, is calculated and compared with the experimental results [10]. However, the triton burnup ratio calculated by GNET is smaller than that measured in the experiments. In GNET, the re-entering particles repeatedly exiting and reentering the last closed flux surface (LCFS) [11, 12] are considered as lost particles because the particle loss boundary is set on the LCFS. Furthermore, the velocity of DD-produced T is assumed to be isotropic in GNET because the momentum of the NB-injected D is ignored at the time of the fusion reaction.

Thus, the final aim of our research is to analyze the confinement and properties of DD-produced T. To achieve this aim, we developed a code to calculate the velocity and spatial profiles of fusion products, based on a Monte Carlo code that has been used for the analysis of neutral beam injection (NBI) heating in LHD and Heliotron-J [13, 14]. In this study, the simulation results of the spatial profile of the fusion products, i.e., the emission rate of NB-driven DD neutrons, are reported.

This study is organized as follows. The outline of the developed code is provided in §2. The results of the test calculation using the developed code are presented in §3. The effect of the impurity ion on the neutron emission rate is shown in §4. A brief summary is provided in §5.

2. Outline of Modified Code

We developed a code to compute the velocity and spatial profile of the fusion products in LHD based on a Monte Carlo code called MORH. In the developed code, a large number of NB-injected D are traced under the influence of Coulomb collision [15] in the real coordinate system. The

author's e-mail: shopon@eng.hokudai.ac.jp

*) This article is based on the presentation at the 30th International Toki Conference on Plasma and Fusion Research (ITC30).

orbit-tracing calculation is stopped when one of the following three conditions is satisfied: (i) orbit loss to the vacuum vessel wall, (ii) charge-exchange loss because of the cold neutrals in the bulk plasma, or (iii) thermalization of the test ion to the temperature of the bulk plasma. The staying time $\delta\tau_i$ in each volume element ΔV_i set in the phase space is calculated during the orbit tracing, where i is the spatial grid numbers. By using $\delta\tau_i$, the fusion reaction rate $S(\boldsymbol{x}_i)$, which represents the spatial profile of the fusion products, is calculated as

$$S(\boldsymbol{x}_i) = \left(\sum_{n=1}^{N} W_n n_{\mathrm{D}}^{\mathrm{BULK}}(\boldsymbol{x}_i) \langle \sigma v \rangle \times \delta\tau_i^n \right) / \Delta V_i, \tag{1}$$

where $W_n = P^{\mathrm{NB}}/E_n^{\mathrm{NB}}$ is the weight of the n-th ion, $n_{\mathrm{D}}^{\mathrm{BULK}}$ the density of the bulk D ion, and $\langle \sigma v \rangle$ the fusion reaction rate coefficient, respectively. Here, P^{NB} is the port-through power of the NB and E_n^{NB} is the initial energy of the NB-injected ion. $S(\boldsymbol{x}_i)$ is the neutron (triton) emission (birth) rate when D(d,n)He^3 (D(d,p)T) is selected as the reaction of $\langle \sigma v \rangle$. Hereafter $S_{\mathrm{n}}(\boldsymbol{x}_i)$ is the neutron emission rate calculated from Eq. (1) using $\langle \sigma v \rangle_{\mathrm{D(d,n)He^3}}$.

The velocity profile of the fusion product under the consideration of the momentum of the NB-injected D can be obtained in three steps: i) calculate the distribution function of the center-of-gravity velocity of the complex nucleus produced when a pair of D ions react, ii) determine the distribution function in the laboratory frame from the distribution function of the center-of-gravity velocity and the distribution function of the velocity of the fusion product in the center-of-mass frame, and iii) produce the velocity of the fusion product in the laboratory frame based on the distribution function obtained in Step ii.

The distribution function of the center-of-gravity velocity of the complex nucleus (F^{CM}) is defined by

$$S(\boldsymbol{x}_i) = n^{\mathrm{NB}} n^{\mathrm{BULK}} \int F^{\mathrm{CM}}(\boldsymbol{x}_i, \boldsymbol{v}^{\mathrm{CM}}) \mathrm{d}\boldsymbol{v}^{\mathrm{CM}}, \tag{2}$$

where $\boldsymbol{v}_k^{\mathrm{CM}}$ is the center-of-gravity velocity of the complex nucleus and n^{NB} and n^{BULK} are the density of NB-injected D ion and D ion in the bulk plasma, respectively. F^{CM} is calculated numerically as

$$F_{\mathrm{CM}}(\boldsymbol{x}_i, \boldsymbol{v}_k^{\mathrm{CM}}) = \left(\sum_{n=1}^{N} W_n F_{\mathrm{CM}}^0(\boldsymbol{x}_i, \boldsymbol{v}_k^{\mathrm{CM}}) \times \delta\tau_{i,k}^n \right) / \Delta V_{i,k}, \tag{3}$$

where F_{CM}^0 is the distribution function of the center-of-gravity velocity for the NB-injected D ion. When the distribution function of the NB-injected D ion is assumed to be the delta function $\delta(\boldsymbol{v}^{\mathrm{NB}} - \boldsymbol{v}_0^{\mathrm{NB}})$ in the laboratory frame and $\boldsymbol{v}_k^{\mathrm{CM}}$ is the center-of-gravity velocity of the complex nucleus in the k-th grid of the center-of-gravity velocity. F_{CM}^0 is obtained by

$$\left(\frac{m_{\mathrm{D}}^{\mathrm{BULK}}}{m_{\mathrm{D}}^{\mathrm{NB}} + m_{\mathrm{D}}^{\mathrm{BULK}}} \right)^3 F_{\mathrm{CM}}^0(\boldsymbol{x}_i, \boldsymbol{v}_k^{\mathrm{CM}}) = \sigma \left| \boldsymbol{v}_0^{\mathrm{NB}} - \boldsymbol{v}^{\mathrm{BULK}} \right| f^{\mathrm{BULK}}(\boldsymbol{x}_i, \boldsymbol{v}_k^{\mathrm{CM}}; \boldsymbol{v}_0^{\mathrm{NB}}). \tag{4}$$

The distribution function of the fusion products in the laboratory frame $f^{\mathrm{FP}}(\boldsymbol{v})$ is determined as

$$f^{\mathrm{FP}}(\boldsymbol{v}) = \int f_0(\boldsymbol{u}) F_{\mathrm{CM}}(\boldsymbol{v}^{\mathrm{CM}}) \mathrm{d}\boldsymbol{u}, \tag{5}$$

where $f_0(\boldsymbol{u})$ is the distribution function of the fusion product in the center-of-mass frame. Here, $\boldsymbol{u}$ and $\boldsymbol{v}$ are the velocity of the fusion product in the center-of-mass and laboratory frame, respectively. For example, the velocity that satisfies f^{FP} can be obtained by rejection sampling.

3. Test Calculation of Developed Code

To validate the developed code, the neutron emission rate was calculated for the two discharges in the LHD experiment, namely, #154892 (ctr-NB) and #154881 (co-NB). The following numerical conditions are used for the validation. The vacuum magnetic field ($R_{\mathrm{ax}} = 3.6\,\mathrm{m}$ and $B_{\mathrm{ax}} = 2.75\,\mathrm{T}$) was used because the plasma beta is low in these two discharges ($\langle\beta\rangle_{\mathrm{dia}} = 0.94\%$(#154892) and 0.60%(#154881)). The density and temperature of electron are given by eighth-degree polynomials based on experimental measurements (Fig. 1). Because a pure-deuterium bulk plasma is assumed, the density of electron is equal to that of the bulk D ion ($n_{\mathrm{D}}^{\mathrm{BULK}}/n_{\mathrm{e}} = 1$). The temperatures of the electron and D are similar. The initial position and velocity of each of the approximately 30,000 NB-injected D ions are obtained by the HFREYA code [16]. P^{NB} was set as 1 MW. The initial energy was assumed as $E_n^{\mathrm{NB}} = 159\,\mathrm{keV}$ for ctr-NB and $E_n^{\mathrm{NB}} = 169\,\mathrm{keV}$ for co-NB. It is noted that the charge-exchange loss is ignored in the present calculation.

Figure 2 shows the numerically obtained neutron emission rate S_{n} on the vertical elongated poloidal plane in LHD. S_{n} in Fig. 2 is normalized by the maximum value ($S_{\mathrm{n}}^{\mathrm{max}} = 0.47$(ctr-NB) and 0.89(co-NB) $\times 10^{14}\,\mathrm{m^{-3}s^{-1}}$). For ctr-NB, the region $S_{\mathrm{n}}/S_{\mathrm{n}}^{\mathrm{max}} \geq 0.75$ widely spreads up to $\rho \simeq 0.4$. S_{n} near the magnetic axis is slightly smaller than that in the surrounding region. However, S_{n} in the case

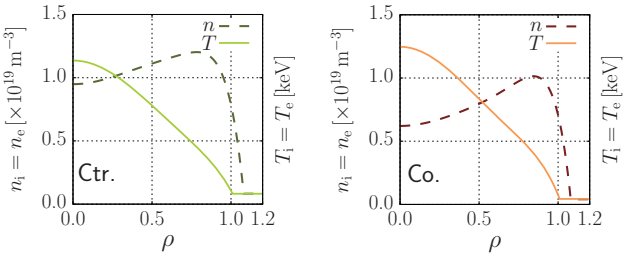

Fig. 1 Bulk plasma density and temperature profile (left: #154892 (ctr-NB) and right: #154881 (co-NB)). The horizontal axis is the averaged minor radius ρ.

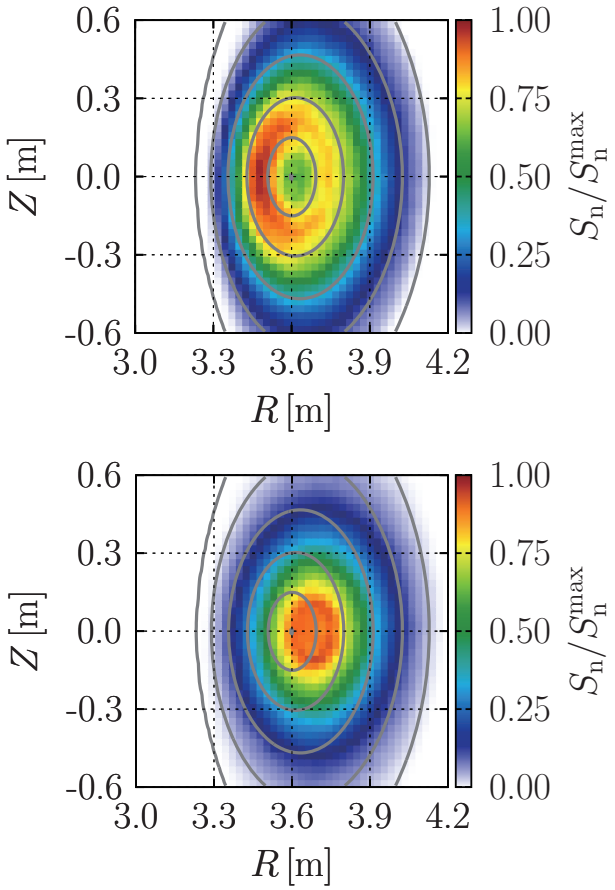

Fig. 2 Neutron emission rate S_n on the vertical elongated poloidal plane (upper: #154892 (ctr-NB) and lower: #154881 (co-NB)). Contour lines of ρ at an interval of $\Delta\rho = 0.2$ are shown for reference. S_n is normalized by the maximum value ($S_n^{max} = 0.47$(ctr-NB) and 0.89(co-NB) $\times 10^{14}$ m^{-3}s^{-1}).

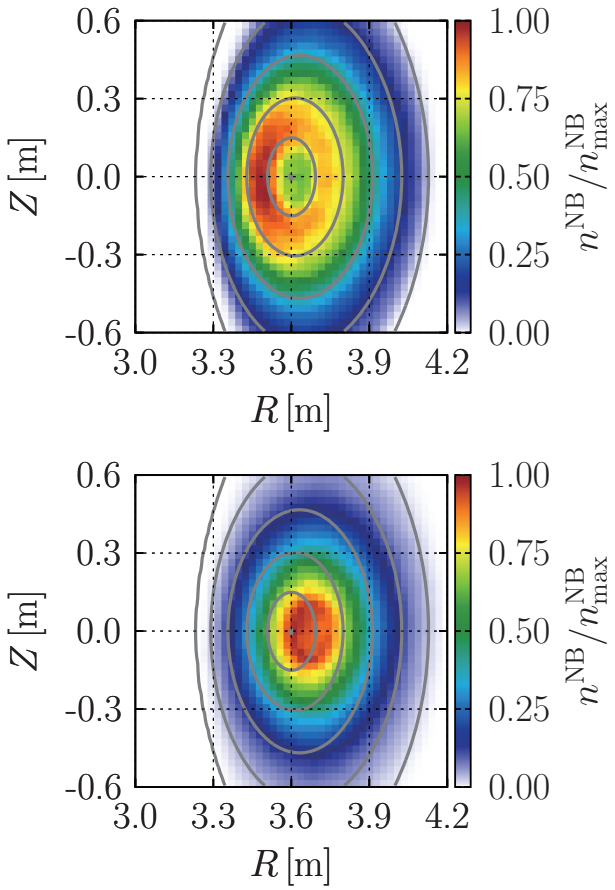

Fig. 3 Density profile of NB-injected D ions ($n^{NB}(\boldsymbol{x})$), which are steadily confined within the vacuum-vessel wall (upper: #154892 (ctr-NB) and lower: #154881 (co-NB)). Contour lines of ρ at an interval of $\Delta\rho = 0.2$ are shown for reference. Densities are normalized by the maximum value ($n_{max}^{NB} = 3.03$ (ctr-NB) and 7.74 (co-NB) $\times 10^{18}$ m^{-3}).

of co-NB has the peaked profile compared with that in the ctr-NB case. Moreover, the maximum S_n value in co-NB case is about twice of that in ctr-NB. The density profile of NB-injected D ions ($n^{NB}(\boldsymbol{x})$) that are steadily confined within the vacuum vessel wall is shown in Fig. 3. $n^{NB}(\boldsymbol{x})$ was calculated as

$$n^{NB}(\boldsymbol{x}_i) = \left(\sum_{n=1}^{N} W_n \delta\tau_i^n\right)/\Delta V_i. \quad (6)$$

It can be seen through comparison of Figs. 2 and 3 that the large S_n area nearly corresponds to the high-$n^{NB}(\boldsymbol{x})$ region because S_n is proportional to $n^{NB}(\boldsymbol{x})$. The volume-integrated S_n in the ctr-NB case was $\overline{S_n^{ctr}} \simeq 3.8 \times 10^{14}$ s^{-1}, and that in the co-NB case was $\overline{S_n^{co}} \simeq 5.0 \times 10^{14}$ s^{-1}. These difference in S_n between the two discharges are primarily attributed to the difference in the orbit property because of the incident direction of the NB.

The neutron counting rate calculated by the line-integration of S_n along the sight lines of the VNC installed in LHD is shown in Fig. 4. The numerically obtained neutron counting rate has similar shape to that of the experimentally measured one. The numerically obtained neutron counting rates in the peripheral region matched the experimental values. However, the rates in the region near the magnetic axis were twice as large as those measured in the experiment. Furthermore, the volume integration of the neutron emission rate in the experiment ($\overline{S_n^{exp}} \simeq 1.5 \times 10^{14}$ s^{-1}) was less than half that obtained by our simulation ($\overline{S_n^{ctr}} \simeq 3.8 \times 10^{14}$ s^{-1} and co-NB: $\overline{S_n^{co}} \simeq 5.0 \times 10^{14}$ s^{-1}).

4. Effect of Impurity on Neutron Emission Rate

As shown in §3, our code overestimated the neutron emission rate S_n. One reason for this difference may be the effect of an impurity ion such as ${}^{1}_{1}$H, ${}^{4}_{2}$He and ${}^{12}_{6}$C. The impurity affects the orbit of NB-injected D through collision and affects the fusion reaction rate through dilution of the density of the bulk D ion. The typical value of the effective atomic number Z_{eff} measured by the extreme ultraviolet spectrometer in the LHD experiment is

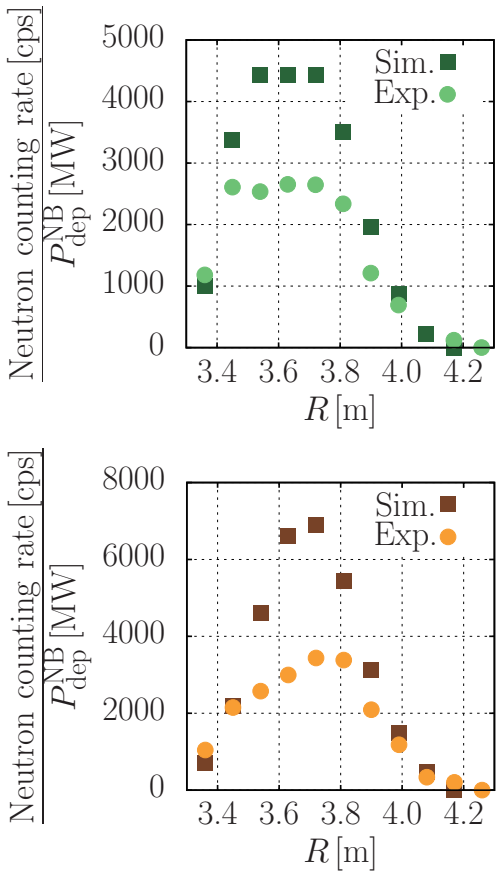

Fig. 4 Neutron counting rate via line integration of $S_{\rm n}$ along the sight lines of the vertical neutron camera (VNC) installed in LHD (upper: #154892 (ctr-NB) and lower: #154881 (co-NB)). Vertical axis is the neutron counting rate normalized by the deposition power of the NB. The experimentally measured value by VNC is shown.

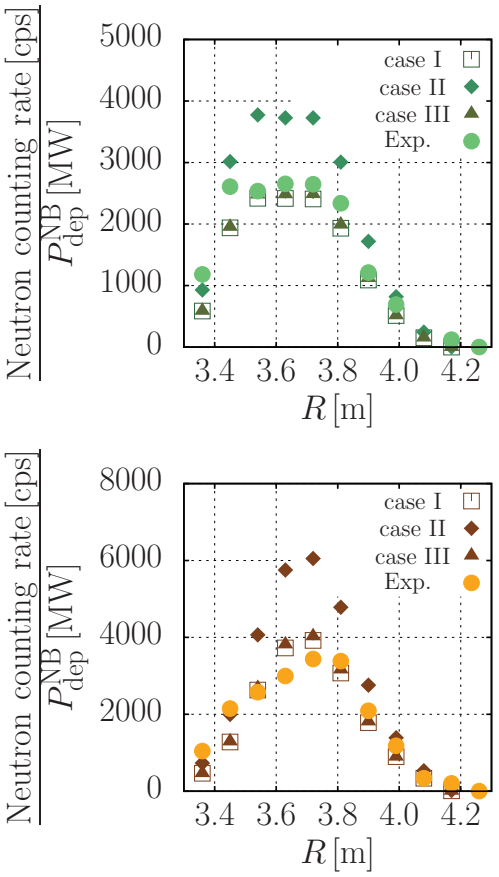

Fig. 5 Neutron counting rate via line integration of $S_{\rm n}$ along the sight lines of the VNC installed in LHD (upper: #154892 (ctr-NB) and lower: #154881 (co-NB)). Vertical axis is the neutron counting rate normalized by the deposition power of NB. The numerical conditions of the bulk plasma (cases I-III) are shown in Table 1. The experimentally measured value is also shown for reference.

Table 1 Numerical condition of the bulk plasma containing the impurity. Here, $R_{\rm d}^{\ell}$ is the density ratio of ℓ-ion defined as $R_{\rm d}^{\ell} \equiv n_{\ell}/n_{\rm e}$.

	impurity	$Z_{\rm eff}$	$R_{\rm d}^{\rm D}$	$R_{\rm d}^{\rm C}$ or $R_{\rm d}^{\rm He}$
case I	C	3.1	0.58	0.07
case II	C	3.1	0.94	0.06
case III	He	1.42	0.58	0.21

Table 2 Volume integration of the neutron emission rate ($\overline{S_{\rm n}}$ [$\times 10^{14}$ s^{-1}]) in three cases of the bulk plasma containing impurity and the ratio of $\overline{S_{\rm n}}$ between with and without impurity.

	ctr-NB		co-NB	
	$\overline{S_{\rm n}}$	$\overline{S_{\rm n}}/\overline{S_{\rm n}^{\rm w/o}}$	$\overline{S_{\rm n}}$	$\overline{S_{\rm n}}/\overline{S_{\rm n}^{\rm w/o}}$
case I	2.1	0.55	2.9	0.58
case II	3.3	0.87	4.5	0.9
case III	2.2	0.58	3.0	0.60
experiment	1.5	0.39	1.5	0.3
w/o impurity	3.8	1.0	5.0	1.0

$2 \lesssim Z_{\rm eff} \lesssim 4$. Here, the effective atomic number is defined as $Z_{\rm eff} \equiv \sum_{\ell} Z_{\ell}^2 n_{\ell}/n_{\rm e}$, where ℓ is the ion species. Thus, we re-calculated $S_{\rm n}$ in three cases of the bulk plasma (Table 1) to investigate the influence of the impurity ion on $S_{\rm n}$. To calculate the density ratio $R_{\rm d}^{\ell}(\equiv n_{\ell}/n_{\rm e})$ in Table 1, we adopted the same electron density profile given by the polynomials listed in §3 and assumed that the impurity atoms are completely ionized. Note that electrical neutrality is satisfied in cases I and III, but not in case II.

Figure 5 shows the neutron counting rate re-calculated using the revised bulk plasma density profile. It can be seen from Fig. 5 that the neutron counting rate in cases I and III are nearly the same as that obtained by the experiment. However, the neutron counting rate in case II is still greater than the experimental value. The volume integration of the neutron emission rate, $\overline{S_{\rm n}}$, is summarized in Table 2. It is confirmed that $\overline{S_{\rm n}}$ approached the experimental value when the impurity was considered. $\overline{S_{\rm n}}$ in case III is approximately equal to $\overline{S_{\rm n}}$ in case I, despite the differ-

ent $Z_{\rm eff}$. However, $\overline{S_{\rm n}}$ in case II, where $Z_{\rm eff}$ is the same as in case I, is greater than that in the other cases. The ratios of $\overline{S_{\rm n}}$ with and without impurity ($\overline{S_{\rm n}}/\overline{S_{\rm n}^{\rm w/o}}$) in Table 2 are nearly the same as $R_{\rm d}^{\rm D}$. These results suggest that the neutron emission rate does not depend on the species of impurity, but strongly depends on the density of the bulk D ion. Moreover, these results indicate that the orbit of NB-injected D ion are not strongly affected by the impurity.

Although $\overline{S_{\rm n}}/\overline{S_{\rm n}^{\rm w/o}}$s are almost the same as $R_{\rm d}^{\rm D}$ in the three cases of the bulk plasma, those by ctr-NB are slightly smaller than those by co-NB. This could be attributed to the difference in the amount of impurities between the two NB cases, as the impurity ion density is given by the multiplication of $R_{\rm d}$ with the electron density, and the electron density differs between ctr-NB and co-NB (see Fig. 1).

In this study, the ion density is assumed to be the multiplication of $R_{\rm d}$ with the electron density profile given by eighth-degree polynomials based on the experimental measurements. Thus, all ions have similar spatial profiles of n_ℓ, because the spatial profile of $n_{\rm e}$ is fixed. It may be possible to set the individual profiles of the ion density. For example, when the density ratio is determined by the radial integration as $[\int_0^1 n_\ell(\rho){\rm d}\rho]/[\int_0^1 n_{\rm e}(\rho){\rm d}\rho]$, if the density profile in $\rho < 0.4$ was largely modified from the profile used in this study, the orbit of the high energy D produced by NBI would be more strongly affected. Consequently, the spatial profile of the neutron emission rate $S_{\rm n}$ would drastically change.

5. Summary

As the first step for the orbit analysis of DD-produced T, in which the particle-loss boundary and velocity anisotropy of T at birth are properly treated, we developed a code to calculate the velocity and spatial profiles of the fusion products in LHD based on the MORH code. The neutron emission rate and the neutron counting rate calculated by the developed code were compared with the experimental results. It was confirmed that the experimental results are reproduced by the developed code when the bulk plasma density including the impurity ion was used.

In this study, the neutron counting rate calculated by the code was still slightly greater than that obtained experimentally. This is because of the difference between the species and spatial profile of the impurity ion. As mentioned above, ${}_1^1$H and ${}_2^4$He, as well as ${}_6^{12}$C, are observed as the impurity ions in the deuterium experiments in LHD. The spatial profile of these impurity ions should be different from those of the electron and D and have a peak in the peripheral region. With the influence of impurity ions, not only is the reaction rate of DD fusion reduced but the orbit of T also changes. Calculations using the impurity density profile based on the experiment will be performed.

We have confirmed the velocity-distribution function of DD-produced T using the code developed in this work. Moreover, orbit analysis of T is ongoing. These results will be presented the near future.

Acknowledgments

The authors wish to thank Prof. S. Tomioka and Prof. Y. Yamauchi for their valuable discussions. The thorough and helpful comments of the reviewer regarding preliminary versions of the article are gratefully acknowledged. The calculations in this study were performed on "Plasma Simulator" (NEC SX-Aurora TSUBASA) of NIFS with the support of and under the NIFS Collaborative Research Program (NIFS21KLPR055 and NIFS21KNSR016).

[1] Y. Takeiri *et al.*, IEEE Trans. Plasma Sci. **46**, 2348 (2018).
[2] M. Osakabe *et al.*, IEEE Trans. Plasma Sci. **46**, 2324 (2018).
[3] Y. Takeiri *et al.*, IEEE Trans. Plasma Sci. **46**, 1141 (2018).
[4] M. Osakabe *et al.*, Fusion Sci. Technol. **72**, 199 (2018).
[5] M. Isobe *et al.*, IEEE Trans. Plasma Sci. **46**, 2050 (2018).
[6] K. Ogawa *et al.*, Nucl. Fusion **58**, 034002 (2018).
[7] S. Murakami *et al.*, Nucl. Fusion **40**, 693 (2000).
[8] S. Murakami *et al.*, Nucl. Fusion **46**, L19 (2002).
[9] S. Murakami *et al.*, Nucl. Fusion **46**, S425 (2002).
[10] K. Ogawa *et al.*, Plasma Phys. Control. Fusion **60**, 9 (2018).
[11] T. Watanabe *et al.*, Kakuyugo Kenkyu **68**, 9 (1992) [in Japanese].
[12] Y. Matsumoto *et al.*, J. Phys. Soc. Jpn. **71**, 1684 (2002).
[13] R. Seki *et al.*, Plasma Fusion Res. **10**, 1402077 (2015).
[14] Y. Matsumoto *et al.*, Proc. ISHW2017, P2-17.
[15] K. Hamamatsu *et al.*, Plasma Phys. Control. Fusion **49**, 1955 (2007).
[16] S. Murakami *et al.*, Trans. Fusion Technol. **27**, 256 (1995).